Diagnosing the contribution of phytoplankton functional groups to the production and export of particulate organic carbon, CaCO₃, and opal from global nutrient and alkalinity distributions

X. Jin,[1] N. Gruber,[1] J. P. Dunne,[2] J. L. Sarmiento,[3] and R. A. Armstrong[4]

[1] We diagnose the contribution of four main phytoplankton functional groups to the production and export of particulate organic carbon (POC), CaCO₃, and opal by combining in a restoring approach global oceanic observations of nitrate, silicic acid, and alkalinity with a simple size-dependent ecological/biogeochemical model. In order to determine the robustness of our results, we employ three different variants of the ocean general circulation model (OGCM) required to transport and mix the nutrients and alkalinity into the upper ocean. In our standard model, the global export of CaCO₃ is diagnosed as 1.1 PgC yr⁻¹ (range of sensitivity cases 0.8 to 1.2 PgC yr⁻¹) and that of opal as 180 Tmol Si yr⁻¹ (range 160 to 180 Tmol Si yr⁻¹). CaCO₃ export is found to have three maxima at approximately 40°S, the equator, and around 40°N. In contrast, the opal export is dominated by the Southern Ocean with a single maximum at around 60°S. The molar export ratio of inorganic to organic carbon is diagnosed in our standard model to be about 0.09 (range 0.07 to 0.10) and found to be remarkably uniform spatially. The molar export ratio of opal to organic nitrogen varies substantially from values around 2 to 3 in the Southern Ocean south of 45°S to values below 0.5 throughout most of the rest of the ocean, except for the North Pacific. Irrespective of which OGCM is used, large phytoplankton dominate the export of POC, with diatoms alone accounting for 40% of this export, while the contribution of coccolithophorids is only about 10%. Small phytoplankton dominate net primary production (NPP) with a fraction of ∼70%. Diatoms and coccolithophorids account for about 15% and less than 2% of NPP, respectively. These diagnosed contributions of the main phytoplankton functional groups to NPP are also robust across all OGCMs investigated. Correlation and regression analyses reveal that the variations in the relative contributions of diatoms and coccolithophorids to NPP can be predicted reasonably well on the basis of a few key parameters.

Citation: Jin, X., N. Gruber, J. P. Dunne, J. L. Sarmiento, and R. A. Armstrong (2006), Diagnosing the contribution of phytoplankton functional groups to the production and export of particulate organic carbon, CaCO₃, and opal from global nutrient and alkalinity distributions, *Global Biogeochem. Cycles*, *20*, GB2015, doi:10.1029/2005GB002532.

1. Introduction

[2] Marine planktonic ecosystems are characterized by great species diversity, yet the processes that maintain such a large number of species are not well understood [cf. *Hutchinson*, 1961]. Given this diversity, it is virtually impossible to develop quantitative models that take this complexity at the taxonomic level into account. From a biogeochemical perspective, this level of detailed description may not be necessary as many species perform similar chemical transformations and respond similarly to changes in their chemical/physical/biological environments. It has become common practice in ecological/biogeochemical modeling to shed considerations on the species composition and focus instead on biogeochemical functional groups (or guilds) [e.g., *Iglesias-Rodriguez et al.*, 2002b; *Moore et al.*, 2002; *Gregg et al.*, 2003]. Functional groups are organisms with common biogeochemical processes; that is, they share the same functional or operational characteristics, or they

[1]Institute of Geophysics and Planetary Physics and Department of Atmospheric and Oceanic Sciences, University of California, Los Angeles, Los Angeles, California, USA.
[2]NOAA Geophysical Fluid Dynamics Laboratory, Princeton, New Jersey, USA.
[3]Atmospheric and Oceanic Sciences Program, Princeton University, Princeton, New Jersey, USA.
[4]Marine Sciences Research Center, Stony Brook University, Stony Brook, New York, USA.

are uniquely associated with the cycling of a particular element [*Iglesias-Rodriguez et al.*, 2002b]. Diatoms and coccolithophorids comprise two of the most important phytoplankton functional groups. Other biogeochemically important functional groups include diazotrophs, nano/picoplankton, and large phytoplankton that are not diatoms.

[3] Phytoplankton functional groups shape the structure of the ecosystem by determining the flow of energy and matter through it. In particular, they control the amount and composition of the organic matter that escapes remineralization in the euphotic zone and is exported to the ocean's interior [*Buesseler et al.*, 1998]. Diatom dominated systems tend to have a high export ratio, i.e., ratio of export to net primary production (NPP). In contrast, picophytoplankton-dominated systems tend to be very inefficient at exporting organic matter from the surface ocean. Because ballast in the form of opal or $CaCO_3$ influences how organic matter settles through the water column and escapes remineralization [*Armstrong et al.*, 2002; *Klaas and Archer*, 2002], phytoplankton community structure is also thought to impact processes in the aphotic zone. The production ratio of organic matter to $CaCO_3$ affects also the air-sea carbon balance owing to their differential impact on the partial pressure of CO_2. Diazotrophs occupy a central role in the marine nitrogen cycle, as their fixation of N_2 represents the most important source of fixed nitrogen to the ocean [*Gruber and Sarmiento*, 1997; *Karl et al.*, 2002; *Gruber*, 2004]. This nitrogen input can be comparable to the upward flux of nitrate into the euphotic zone by upwelling, diffusion and mixing [*Capone et al.*, 2005] and in certain regions may fuel a substantial fraction of export production.

[4] Some pioneering oceanic ecological models have begun to include this diversity explicitly [*Moore et al.*, 2002; *Gregg et al.*, 2003]. While these models tend to capture the expected distribution of the major phytoplankton functional groups, there are very few observations available to evaluate their results.

[5] In situ observations of phytoplankton functional group abundances are scarce and often incomplete because only a few groups were usually considered. With the recent application of high-performance liquid chromatography (HPLC), pigment approaches and flow cytometry, information of phytoplankton functional group abundances and distributions are increasing [*Gregg et al.*, 2003; *Gibb et al.*, 2000; *Veldhuis and Kraay*, 2004]. Nevertheless, the constraints from in situ observations are still weak.

[6] Although much effort has been spent to use satellite observations to estimate phytoplankton functional groups, this avenue remains challenging. This is mainly a result of the light absorption and reflectance properties of different phytoplankton functional groups being so similar, making their detection and quantification difficult. Some progress has been made with regard to a few functional groups, for example, coccolithophorids [*Brown and Yoder*, 1994; *Gordon et al.*, 2001; *Iglesias-Rodriguez et al.*, 2002b], *Trichodesmium* [*Subramaniam et al.*, 2002] and diatoms [*Sathyendranath et al.*, 2004]. However, in most cases, only full bloom conditions can be detected, which provides limited constraints for model evaluation.

[7] An alternative approach is to exploit observations of nutrients and alkalinity, as their distribution contains information about the production and export of organic carbon, $CaCO_3$ and opal, and thereby implicitly contain information about the main phytoplankton functional groups. *Najjar et al.* [1992] were among the first to follow this idea by employing a phosphate restoring approach to diagnose the export of organic matter. Such a restoring approach has been used in many subsequent studies, including the second phase of the Ocean Carbon Model Intercomparison Project (OCMIP) [e.g., *Najjar and Orr*, 1998]. *Gnanadesikan* [1999] extended this method to silicic acid permitting him to diagnose the export of opal. More sophisticated methods to use nutrient observations to determine biological production have been introduced recently, such as inverse modeling with the adjoint technique [e.g., *Schlitzer*, 2002; *Usbeck et al.*, 2003]. However, most of these studies focused so far on the production and export of only one component of the biogenic production and export of particulate matter and did not take advantage of the information contained in these data about phytoplankton functional groups.

[8] Our aim here is to combine the information from all tracers and estimate the contribution of four main phytoplankton functional groups (diatoms, large nondiatom phytoplankton, coccolithophorids, and small noncoccolithophorid phytoplankton) to the production and export of organic carbon, $CaCO_3$ and opal. We are also interested to determine the factors that control the relative contribution of these functional groups to NPP and the export of particulate organic carbon (POC). We are particularly interested in what determines the fraction of large phytoplankton production that is undertaken by diatoms, and in what determines the fraction of small phytoplankton production that is undertaken by coccolithophorids. One of our motivations for the determination of these allocation fractions is the longer-term goal of developing a simplified semiprognostic model of phytoplankton functional groups, but one whose parameterizations are well constrained by observations.

[9] We tackle our main aim by following the classical restoring approach for the determination of the export of $CaCO_3$ and opal, but use a simple ecological/biogeochemical model developed by J. P. Dunne et al. (Diagnosed primary production, export and size structure in a global ocean general circulation model, manuscript in preparation, 2006) (hereinafter referred to as Dunne et al., manuscript in preparation, 2006) to determine NPP and the export of POC and dissolved organic carbon (DOC). This latter model is also based on the restoring of simulated nitrate toward observations, but it includes the explicit cycling of ammonia and dissolved organic nitrogen, as well as the separation of the phytoplankton into two distinct size classes, i.e., pico/nanoplankton (nominally <5 μm), and large phytoplankton (Dunne et al., manuscript in preparation, 2006). This simple model has been extensively calibrated against a large set of observations of particle export ratios [*Dunne et al.*, 2005]. The model's primary relevance beyond the estimation of NPP and the separation of the phytoplankton into a small and large size classes is to establish the partitioning of organic matter into DOC and POC. The ecosystem model is

nitrogen based and since this version does not include nitrogen fixation, we employ a constant stoichiometric C:N ratio of 117:16 to convert organic nitrogen to organic carbon. A version with N_2 fixation (C. Deutsch et al., Oceanic N_2 fixation diagnosed from nutrient distributions, submitted to *Nature*, 2006) shows insignificant changes with regard to the results reported here. With these elements and some assumptions about the fraction of $CaCO_3$ and opal produced in the upper ocean that is exported, we can then determine the relative contribution of the four phytoplankton functional groups considered to NPP and POC export.

[10] In the next section, we describe briefly the model, the data and the experimental design. We then discuss the diagnosed $CaCO_3$ and opal export, and compare them to independent estimates. Subsequently, we combine these export estimates with the organic carbon export estimates from the ecological/biogeochemical model to determine the export ratios, i.e., ratios of opal and $CaCO_3$ export to organic carbon export. Finally, by making assumptions about the export fraction for $CaCO_3$ and opal, as well as for the stoichiometric ratios between organic carbon and $CaCO_3$ and opal, respectively, we determine the contribution of the different functional groups to NPP in the euphotic zone and POC export. An outlook is provided at the end.

2. Methods

[11] Our approach requires three components: an ocean circulation model to provide the oceanic transport and mixing fields, an ocean ecological/biogeochemical (BGC) model to estimate NPP and the export of organic matter, and observations to which the model's simulated tracer fields are restored to. Auxiliary material[1] provides the details, while a summary is given here.

[12] We use three variants of a seasonal coarse-resolution 3-D ocean general circulation model (OGCM) developed at Princeton University on the basis of the Modular Ocean Model (MOM) (see *Gnanadesikan et al.* [2004] for further details). Our standard model, named Princeton 2A (P2A), distinguishes itself from the others primarily by its superior agreement with a range of observational constraints, including radiocarbon and chlorofluorocarbons (CFC) [*Matsumoto et al.*, 2004]. The other two variants of the OGCM, HH and LL, have similar base configurations as P2A, but differ substantially in terms of their explicit mixing parameters, with HH employing high vertical and along-isopycnal mixing coefficients and LL having low vertical and along-isopycnal mixing coefficients. Detailed comparisons of these three models with observations [*Gnanadesikan et al.*, 2002, 2004] and other models [*Matsumoto et al.*, 2004] reveal that they span a large range of behavior exhibited by the current generation of coarse-resolution global OGCMs. However, only HH and P2A simulate CFC and radiocarbon distributions that are consistent with observations, while LL falls outside the observational constraints [*Gnanadesikan et al.*, 2004; *Matsumoto et*

al., 2004]. We consider the results from our P2A simulation as our most trustworthy and use the results from the other two OGCMs to determine the robustness of our results to potential biases arising from the modeled circulation.

[13] The biogeochemical model used to determine organic carbon production and export is based on the two size-class phytoplankton model of Dunne et al. (manuscript in preparation, 2006) (see auxiliary material for the equations of the model). NPP in the model consists of nitrate and ammonia based productions, which are calculated by restoring modeled nitrate to monthly observations from the World Ocean Atlas 2001 (WOA01) database [*Conkright et al.*, 2002] with a timescale of 1 month and by restoring modeled NH_4^+ to zero with a timescale of 3 days. NPP is then allocated to large and small phytoplankton production according to an allometric equation. The small and large phytoplankton are subject to growth and loss due to grazing, to production of detritus, production of dissolved organic nitrogen (DON), and conversion to NH_4^+. Unprotected detritus, i.e., detritus that is not associated with minerals, is subject to remineralization in the euphotic zone, while the remainder is exported.

[14] The export of opal and $CaCO_3$ are diagnosed by restoring silicic acid and salinity normalized potential alkalinity (PAlk) in the euphotic zone to observations with a timescale of 3 months. PAlk is defined as [*Brewer et al.*, 1975]

$$PAlk = (Alk + \mathrm{NO_3}) \cdot \frac{35}{S}, \qquad (1)$$

where S is salinity. Monthly observations for silicic acid were also obtained from the WOA01 database, while we used the annual mean climatology of *Key et al.* [2004] for alkalinity. The model computes salinity normalized potential alkalinity only locally from the model's tracer fields alkalinity, salinity, and nitrate. This avoids many of the problems associated with salinity normalizations [e.g., *Friis et al.*, 2003; *Robbins*, 2001]. Relative to nitrate and silicic acid, which are based on extensive climatologies, the employed alkalinity distribution has much larger uncertainties, mostly because of the limited amount of data that are available to produce global alkalinity maps. In addition, there exist nonnegligible accuracy issues with the measurement of alkalinity [*Lamb et al.*, 2002]. These uncertainties in the data can get aggravated in our diagnostic study by model transport errors, potentially leading to substantial biases in our $CaCO_3$ export estimates. A good indication of these limitations in the diagnostic method is the occurrence of negative restoring terms, i.e., situations in which the model's surface nutrient or salinity normalized potential alkalinity concentration is below the observed concentration. In these situations, we usually set the restoring term to zero. In order to test the robustness of our results to such data-driven uncertainties, we will evaluate also a sensitivity case where we permit negative restoring terms (referred to as P2A-neg). This will lead to negative production and export of the respective terms, i.e., net remineralization or dissolution in the euphotic layer.

---

[1]Auxiliary material is available at ftp://ftp.agu.org/apend/gb/ 2005gb002532.

Table 1. Global Values of Model Diagnosed Oceanic Production, Export, and Rain Ratio[a]

Standard Case P2A Model		Sensitivity Case		
		HH Model	LL Model	P2A-neg Model
NPP, Pg C yr^{-1}	78	96	73	71
POC export, Φ_{POC}, Pg C yr^{-1}	9.8	11.3	8.6	9.4
DOC export, Pg C yr^{-1}	2.9	3.8	2.6	2.7
Organic carbon export, Pg C yr^{-1}	12.7	15.0	11.2	12.1
Opal export, Φ_{SiO_2}, Tmol Si yr^{-1}	178	156	102	172
CaCO$_3$ export, Φ_{CaCO_3}, Pg C yr^{-1}	1.14	1.20	1.08	0.82
C_{inorg}:C_{org} rain ratio	0.090	0.080	0.096	0.068

[a]P2A, HH, and LL refer to three configurations of the ocean general circulation model considered, with P2A representing our standard model, and HH and LL representing two sensitivity cases with high and low mixing, respectively. P2A-neg is the P2A model, but includes negative restoring terms for all elements.

[15] Since the focus of our study here is on the upper ocean, we forgo explicit modeling of the remineralization and dissolution processes in the aphotic zone, i.e., below 75 m, and instead restore model simulated nutrients and potential alkalinity to observations. This ensures that the nutrient concentrations in the aphotic zone are close to the observations and are supplied in the correct ratios to the euphotic zone by the OGCM.

[16] The model does not explicitly consider rivers, which deliver nutrients and alkalinity to the ocean and hence alter the global balance of these tracers. Nevertheless, the effect of rivers is implicitly included in our diagnostic study. This is because the riverine input is reflected in the observed distribution of the nutrients and alkalinity, which is then used as a restoring boundary conditions.
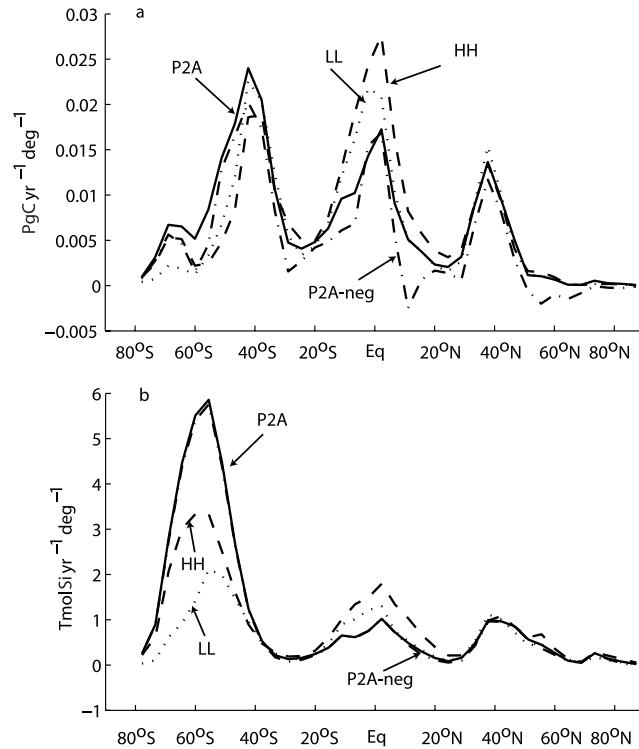
3. Results

3.1. CaCO$_3$ Export

[17] The global CaCO$_3$ export diagnosed by the standard model (P2A) is 1.1 Pg C yr^{-1}, with little sensitivity to modeled transport, but substantial uncertainty with regard to data uncertainties implied by negative restoring terms

Table 2. Summary of Pelagic CaCO$_3$ and Opal Flux Estimates

| Authors	Methods	Flux
CaCO$_3$ Export, PgC yr^{-1}		
This study (Standard)	3-D model (diagnostic)	1.1
Murnane et al. [1999]	3-D model (prognostic)	1.8
Heinze et al. [2003]	3-D model (prognostic)	1.6
Moore et al. [2004]	3-D model (prognostic)	0.5
Sarmiento et al. [2002]	Geochemical	0.6
Lee [2001]	Geochemical	1.1
Li et al. [1969]	Geochemical	0.7
Milliman and Droxler [1996]	after *Li et al.* [1969]	0.7
Opal Export, Tmol Si yr^{-1}		
This study (Standard)	3-D model (diagnostic)	178
Usbeck [1999]	3-D model (inverse)	200
Heinze et al. [2003]	3-D model (prognostic)	185
Gnanadesikan [1999]	3-D model (diagnostic)	89
Nelson et al. [1995]	Geochemical	120

Figure 1. Zonal integral of the model diagnosed export of (a) CaCO$_3$ and (b) opal in the standard model (P2A) and in the three sensitivity cases (HH, LL, and P2A-neg).

(Table 1). The total range of our diagnostic results is 0.8 to 1.2 PgC yr^{-1}.

[18] Existing estimates of CaCO$_3$ export range from 0.5 to 2.0 PgC yr^{-1} (see summary by *Iglesias-Rodriguez et al.* [2002a] and *Feely et al.* [2004], and Table 2). More recent estimates of CaCO$_3$ export based on alkalinity observations give a narrower range of 0.6–1.4 PgC yr^{-1}. By combining observations of the vertical gradients of potential alkalinity and nitrate with an estimate of export production, *Sarmiento et al.* [2002] estimated a CaCO$_3$ export of 0.6 PgC yr^{-1}. From an inventory of alkalinity and the residence time of various water masses, *Milliman and Droxler* [1996] inferred a CaCO$_3$ export of 0.7 PgC yr^{-1}, while *Lee* [2001] recently gave a higher estimate of 1.1 PgC yr^{-1} based on the seasonal cycle of potential alkalinity in the surface mixed layer. Our estimate agrees well with these more recent estimates of global pelagic CaCO$_3$ export.

[19] The zonally integrated CaCO$_3$ export (Figure 1a) shows three well-developed maxima located at around 40°S, the equator, and around 40°N, respectively. Figure 2a illustrates the spatial distribution of the annual mean CaCO$_3$ export in more detail. It reveals that the strong CaCO$_3$ export maximum at around 40°S is a circumpolar phenomenon. It also shows that most of the CaCO$_3$ export in the region north of 40°N stems from the North Pacific, with a relatively small contribution from the North Atlantic.

[20] Our diagnosed large export flux of CaCO$_3$ in the Southern Ocean between about 40°S and 60°S is consistent with sediment trap results [*Milliman*, 1993; *Honjo et al.*, 2003], since they also show a clear export band along about
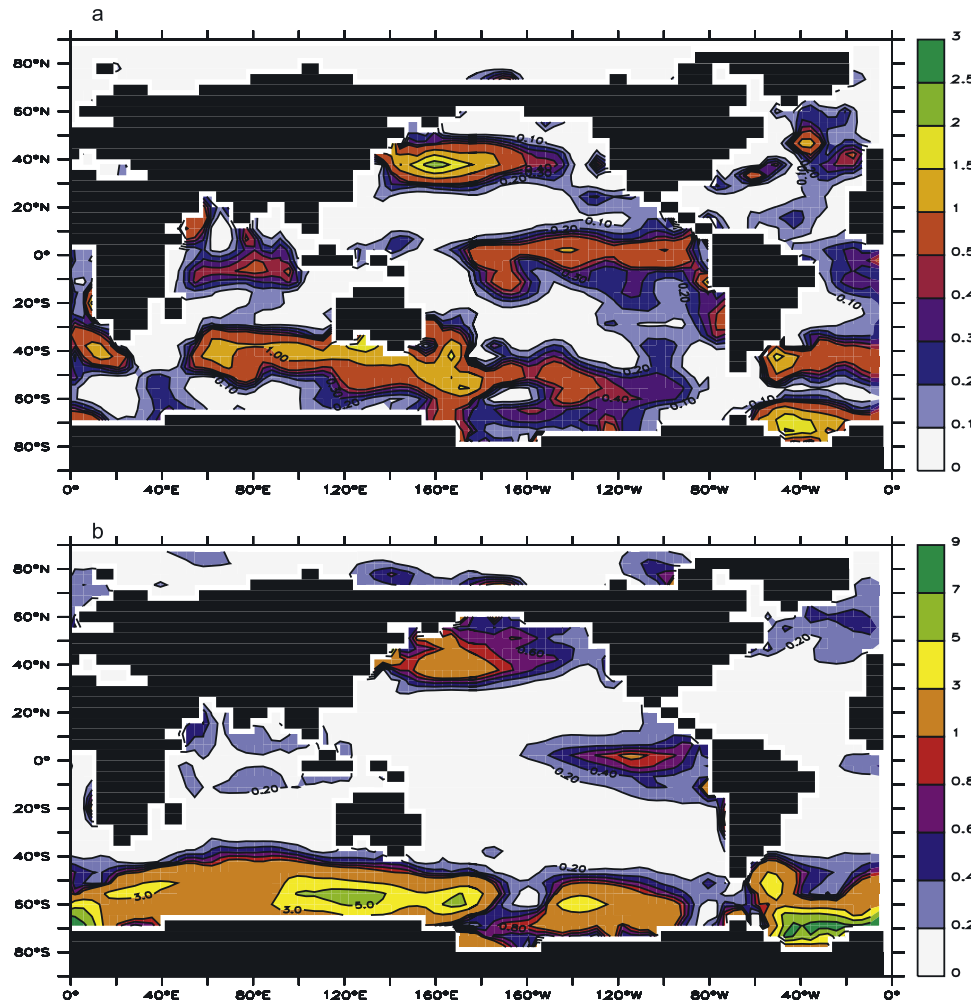
Figure 2. Maps of diagnosed annual mean export of (a) $CaCO_3$ (mol C m^{-2} yr^{-1}) and (b) opal (mol Si m^{-2} yr^{-1}). Shown are the results from the standard model (P2A).

50°S. Satellite estimates [*Brown and Yoder*, 1994; *Iglesias-Rodriguez et al.*, 2002b; *Balch et al.*, 2005] also find high concentrations of suspended $CaCO_3$ in the Southern Ocean, usually interpreted to represent coccolithophorid blooms. Unfortunately, few in situ observations exist to corroborate the existence of large numbers of calcifying coccolithophorids in the Southern Ocean, but the few existing data tend to support this conclusion (W. M. Balch, personal communication, 2005). Some fraction of the $CaCO_3$ export flux in the high latitudes may be driven also by pteropods [*Honjo et al.*, 2000; *Collier et al.*, 2000], which have been shown to dominate the downward $CaCO_3$ flux in the Ross Sea.

[21] The high $CaCO_3$ export in the tropics and northern high latitudes in our standard model is also found in these existing estimates. However, the most recent satellite-based estimate of the distribution of the $CaCO_3$ abundance by *Balch et al.* [2005] gives a distribution that is spatially remarkably uniform without the large maxima seen in our diagnosed fluxes. This difference may be real, however, because spatial differences in $CaCO_3$ turnover times (e.g., faster in upwelling areas) and variations in the fraction of

$CaCO_3$ that escapes dissolution before being exported can decouple the pattern of $CaCO_3$ stock and export. As a result, this comparison remains qualitative.

[22] A more quantitative comparison can be undertaken with the estimates of *Lee* [2001]. The meridional breakdown of $CaCO_3$ export in his estimates and our standard model are: 0.44 versus 0.39 PgC yr^{-1}, south of 40°S; 0.44 versus 0.67 PgC yr^{-1}, between 40°S and 40°N; and 0.24 versus 0.08 PgC yr^{-1}, north of 40°N. Note that *Lee* [2001] was not able to estimate $CaCO_3$ export reliably in the tropics, as the absence of seasonal variability in this region precluded him from applying his technique. Our meridional breakdown agrees reasonably well with Lee's estimates (see also Figure 1a), except for the region north of 40°N, where our estimate is much lower.

[23] Most of the discrepancy for the region north of 40°N stems from the North Atlantic, where our diagnosed export is surprisingly low, given the high abundance of coccolithophorid blooms in this region [*Brown and Yoder*, 1994]. Our use of annual mean data for alkalinity plus the other uncertainties in the alkalinity data stemming from poor

coverage may bias our diagnostic results. Furthermore, vertical gradients in potential alkalinity in the North Atlantic are very small, so that any accuracy issues with the data have a particularly large impact. The potential for data-driven biases in our diagnostic estimate is illustrated by the fact that a simulation that includes the negative production terms generates particularly large negative restoring terms in this region (not shown).

[24] On the other hand, *Lee*'s [2001] approach may overestimate $CaCO_3$ export at high northern latitudes, because he used the seasonal cycle of temperature to estimate the seasonal cycle of potential alkalinity. This is clearly inconsistent with observations from the subtropical gyres [*Bates et al.*, 1996a, 1996b; *Keeling et al.*, 2004]. Finally, it is possible that only a small fraction of the $CaCO_3$ produced in the coccolithophorid blooms in the North Atlantic gets exported.

[25] While the global $CaCO_3$ export shows limited sensitivity to the choice of circulation model (Table 1), there exist some differences with regard to the relative weighting of the various latitude bands (Figure 1a). Relative to the standard model, P2A, the high-mixing model, HH, shifts the zone of maximum zonally integrated export from the Southern Ocean to the tropics, while the low-mixing model, LL, diagnoses an approximately equal contribution between the tropics and the Southern Ocean. All three models have similar magnitudes in the northern latitudes, however.

[26] The sensitivity case that includes negative restoring follows the pattern of the standard case, but is consistently lower, leading to a 28% reduction in global $CaCO_3$ export. This reduction is a direct consequence of our consideration of negative production and export of $CaCO_3$ in this case. We do not interpret this as evidence for actual net dissolution of $CaCO_3$, but rather as an indication of the limitation of the diagnostic method and the currently available alkalinity data.

3.2. Opal Export

[27] The global opal export diagnosed in the standard model (P2A) is 178 Tmol Si yr^{-1} (Table 1). In contrast to $CaCO_3$ export, our diagnosed opal export is highly sensitive to which model is used, but it seems to depend little on uncertainties in the data, as evidenced by the small change in the results if regions of negative restoring are included. The total range of our diagnostic results is 102 to 178 Tmol Si yr^{-1}, but as discussed above, the results from the LL model are likely incorrect, as this model is inconsistent with several data constraints. The more likely range is 156 to 178 Tmol Si yr^{-1}. We subsequently focus on the standard results from the P2A model.

[28] *Nelson et al.* [1995] estimated an opal production of 200–240 Tmol Si yr^{-1} with half of it, 100–140 Tmol Si yr^{-1}, being exported from the euphotic zone. This would suggest that our standard estimate is too large. However, a much higher opal production than suggested by older estimates was recently observed in the Southern Ocean [*Pondaven et al.*, 2000; *Nelson et al.*, 2002]. This new observational result and the fact that the Southern Ocean is by far the biggest contributor to global opal export make our relatively high opal export estimate feasible. This conclu-

sion is supported by two other recent modeling studies. Using an inverse approach that combines data with models, *Usbeck* [1999] estimated a global opal export of about 200 Tmol Si yr^{-1}, and *Heinze et al.* [2003] simulated an opal export of 185 Tmol Si yr^{-1} on the basis of a prognostic calculation.

[29] The zonally integrated opal export (Figure 1b) shows that global opal export is dominated by the Southern Ocean, with a maximum around 60°S. The opal export from 80°S to 40°S accounts for 70% of the total opal export, while the opal export between 40°S to 40°N, and north of 40°N, accounts for 21% and 9%, respectively.

[30] The spatial distribution of opal export diagnosed by the model (Figure 2b) captures the main features of what are known about opal export based on sediment trap data, sediment accumulation data, and other direct observations [*Ragueneau et al.*, 2000; *Honjo et al.*, 2003]. Diagnosed opal export is high throughout the Southern Ocean with values up to 10 mol Si m^{-2} yr^{-1}. The high opal export fluxes are confirmed by the sediment trap observations of *Honjo et al.* [2003] and the very high accumulation rates of opal in the sediment underlying this region. Consistent with in situ observations and opal sediment data, model diagnosed opal export is also elevated in the eastern tropical Pacific Ocean and the North Pacific Ocean, as well as some of the other low- and mid-latitude upwelling areas. The opal export in the Atlantic Ocean is smaller than in the Pacific Ocean, as expected from its much lower subsurface $Si(OH)_4$ concentrations.

[31] The dominance of the Southern Ocean for opal export becomes even more evident by comparing it to $CaCO_3$ export (Figure 1a). In addition, there exists a distinct latitudinal separation in the Southern Ocean maxima with the opal export maximum occurring about 10° farther south than the $CaCO_3$ export maximum.

[32] The high sensitivity of the diagnosed opal export to the choice of circulation model requires some explanation, particularly since the standard model (P2A) is at the high end relative to the low- and high-mixing models. The differences between the models are particularly accentuated in the Southern Ocean, where the export in the standard model (P2A) is 3 times as high as the low-mixing model and 2 times as high as the high-mixing model (Figure 1b). These model differences are directly linked to the magnitude of vertical mixing, with the high-mixing model supplying much more $Si(OH)_4$ to the near surface ocean, requiring a larger export of opal in our diagnostic framework. However, our standard model has the highest opal export in the Southern Ocean despite the fact that its specified mixing is in between that of the high and low-mixing models. This is because the stronger winds in the Southern Ocean in the P2A model lead to a substantial increase in the overturning circulation in this region and the other differences between P2A and the two other models, such as the different topography and the salinity restoring, may also contribute to this (see auxiliary material for model details).

[33] The very different sensitivity of $CaCO_3$ and opal export to changes in the circulation model can be explained by their differing export pattern. Opal export occurs mainly
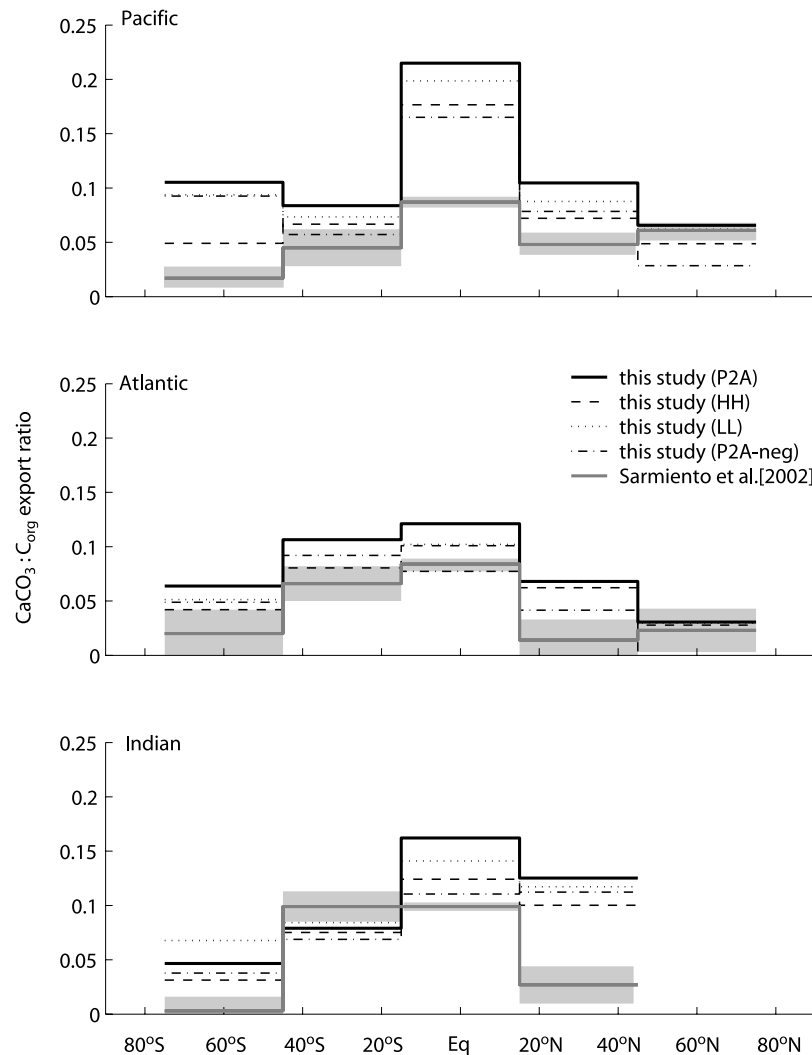
Figure 3. Zonal averages of the $CaCO_3$ to organic carbon export ratio (rain ratio) for each ocean basin. Shown are the results of our models in comparison with the gradient ratio results obtained by *Sarmiento et al.* [2002].

in the Southern Ocean, where the circulation models differ the most, resulting in a large sensitivity of opal export to differences in circulation models. In the case of $CaCO_3$, the distribution of export is more uniform and since the between-model difference in ocean circulation is smaller outside the Southern Ocean, the impact of these differences on the diagnosed export is more modest.

[34] There is little indication of data biases influencing our results, as the inclusion of negative restoring terms in the P2A-neg sensitivity case has a negligible impact on both global as well as regional estimates of opal export. This is likely because the WOA01 database used to produce the silicic acid climatology has a very good spatial and temporal coverage, and also resolves the vertical gradients much better than the very limited alkalinity data base.

3.3. Export Ratios

[35] The global mean export ratios of $CaCO_3$ to organic carbon, i.e., rain ratio, in our standard model is 0.09. This ratio is moderately sensitive to the employed circulation model, but quite sensitive to how negative restoring terms are handled (Table 1). The total range of our solutions is 0.07 to 0.10.

[36] This agrees well with the recent estimates of 0.06 ± 0.03 on the basis of an analysis of vertical gradients of nitrate and potential alkalinity [*Sarmiento et al.*, 2002], and 0.11 on the basis of potential alkalinity data in the mixed layer [*Lee*, 2001]. We can compare our export rain ratio estimate also with the recent estimate of the ratio of the standing stocks of particulate organic carbon (POC) and $CaCO_3$ in the euphotic zone by *Balch et al.* [2005]. They reported a value of 0.05 ± 0.01, which we consider compatible with our export rain ratio estimate of 0.09, since we expect the export ratio to be somewhat larger than the ratio of the standing stocks, as a larger fraction of POC tends to get remineralized before being exported relative to $CaCO_3$.
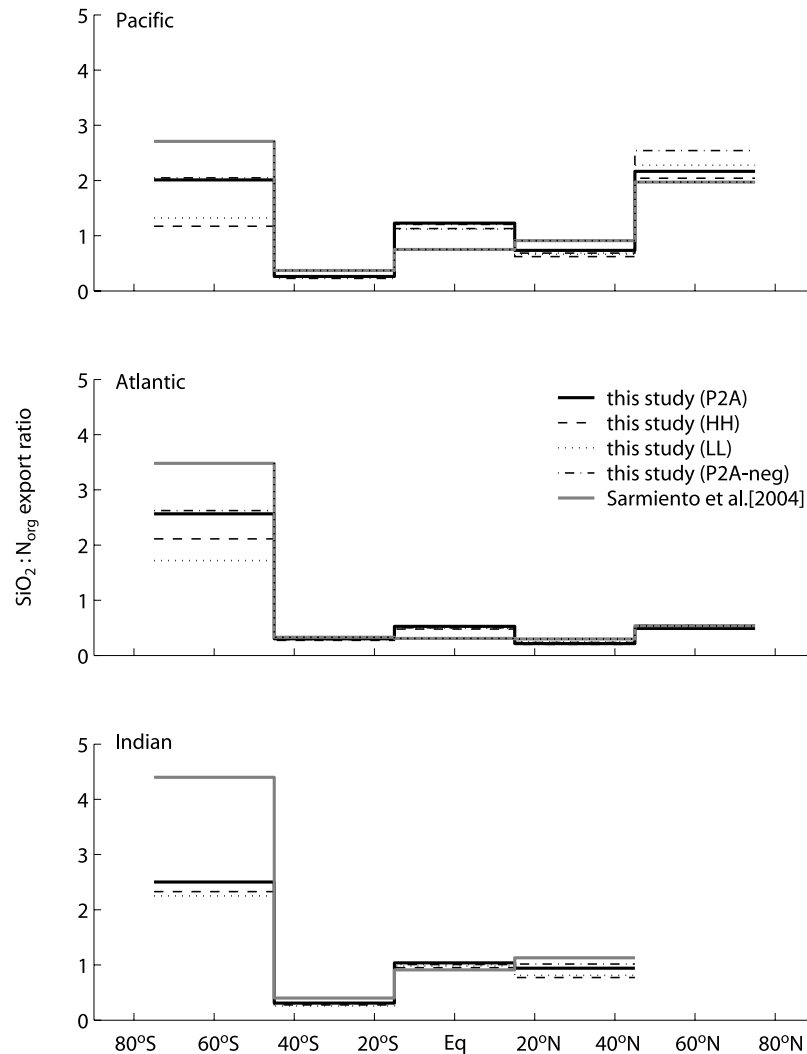
Figure 4. Zonal averages of the opal to organic nitrogen export ratio for each ocean basin. Shown are the results of our models in comparison with the results obtained by *Sarmiento et al.* [2004a].

[37] Our diagnosed export rain ratios exhibit noticeable spatial variations with generally higher values in the tropics and subtropics and lower values in the high latitudes (Figure 3). The highest export rain ratio is found in the tropical Pacific. Our diagnosed ratios have a similar pattern to those estimated by *Sarmiento et al.* [2002], but are, on average, somewhat higher and show a larger amplitude.

[38] The differences between the export rain ratios diagnosed here and those of *Sarmiento et al.* [2002] must come primarily from differences in methodology, since the data sets used in both studies are similar. Although the meridional variations in our rain ratio estimates are relatively insensitive to which circulation model is employed, the diagnosed ratios are consistently lower and more consistent with those of *Sarmiento et al.* [2002] when negative production is permitted to occur (Figure 3). This points

toward considerable uncertainties in our rain ratio estimates stemming from data errors.

[39] On the other hand, the estimates of *Sarmiento et al.* [2002] may be biased low because of their vertical gradient method neglecting horizontal transport processes, and because their mean ratios were computed by area-weighted averaging rather than flux-weighted averaging. In order to test these hypotheses, we reevaluated the gradient-ratio method of *Sarmiento et al.* [2002] using synthetic data from our model. We find that the gradient method tends to underestimate the export rain ratio in the Southern Ocean and the tropics and may be biased either way in other regions. This possible error structure of the gradient-ratio method explains at least part of the difference between our estimate and that of *Sarmiento et al.* [2002]. In the tropics and subtropics, the most likely source of the error in the gradient ratio method is the dynamics of dissolved organic

	Zonal	10°x10°	ICE	SP	ST–SS	ST–PS	LL–U	Eq–U	Eq–D
S	(44)	18	41	21	–22	(–3)	(11)	(4)	(–8)
T	(0)	(2)	(–8)	36	–16	–36	–23	–50	(27)
PO_4	(42)	30	55	(5)	27	54	55	66	(40)
NO_3	50	30	51	(7)	18	56	50	62	(24)
$Si(OH)_4$	(43)	28	69	(3)	16	35	49	48	(26)
$PAlk$	(28)	15	49	(2)	19	45	18	26	(2)
NPP	66	59	63	49	66	51	72	51	(34)
NPP_L	79	60	62	43	65	57	75	52	(28)
NPP_S	47	51	63	56	65	42	64	49	(36)
Chl	53	45	65	26	55	61	73	54	(30)
Φ_{Si}	(46)	42	74	25	43	63	70	70	51
Φ_{POC}	68	54	66	36	62	60	74	55	(28)
Φ_{Corg}	73	55	64	39	61	51	66	54	(–5)
$\Delta N/\Delta t$	(34)	45	64	41	37	29	53	36	(–5)
Z_m	53	41	69	11	39	(0)	(–2)	–27	(–24)
ΔZ_{mld}	51	16	40	(3)	25	58	(–9)	–29	(–28)
E_{cr}	(3)	(–7)	(5)	(7)	–21	–16	(–5)	–22	(3)

Figure 5. Correlation coefficients ($\times100$) between diagnosed $CaCO_3$ export and 17 independent variables for the different aggregations considered. Numbers shown in parentheses are not significant at the 95% significance level using a t-test. The biomes considered are: ice, marginal sea ice; SP, subpolar; ST-SS, subtropical seasonal; ST-PS, subtropical permanent; LL-U, low-latitude upwelling; Eq-U, upwelling; and Eq-D, downwelling (see *Sarmiento et al.* [2004b] and auxiliary Table S2 for further details).

carbon (DOC), which can lead to a substantial spatial decoupling between upward supply and vertical export. In the Southern Ocean, we suspect that strong meridional transports is the cause for the decoupling.

[40] Our reevaluated error structure for the gradient-ratio method is somewhat larger and different than that reported by *Sarmiento et al.* [2002] on the basis of an analysis of synthetic data from a different ocean biogeochemistry model. We suspect that this difference is due to their using synthetic data from a model that has a nearly uniform spatial distribution of the rain ratio, while we used a model with spatially varying rain ratio.

[41] Given the considerable uncertainties in the estimated meridional distribution of the rain ratio in both our diagnostic approach and the gradient-ratio method, it is currently not possible to decide which method is more accurate. However, both methods agree clearly that the rain ratio is much smaller than used in many modeling studies in the past (see discussion by *Sarmiento et al.* [2002]).

[42] The export ratio of opal to organic nitrogen, $SiO_2:N_{org}$, shown in Figure 4 varies much more strongly with latitude than the rain ratio (see Figure 3). In the Southern Ocean the $SiO_2:N_{org}$ export ratio is diagnosed to be between 2 and 3, while values as low as 0.2 are found throughout most of the Atlantic Ocean. Our diagnosed spatial pattern agrees generally well with that reported by *Sarmiento et al.* [2004a], who used the same vertical gradient method *Sarmiento et al.* [2002] employed for determining the export rain ratio. The only regions with significant differences are the Southern Ocean, where the gradient method

estimates larger $SiO_2:N_{org}$ export ratios, and the tropics, where the gradient method yields lower estimates. As uncertainties stemming from possible biases in models and data appear to have almost no effect on our estimate of the $SiO_2:N_{org}$ export ratio (Figure 4), we suspect that these differences are mostly caused by the gradient method neglecting horizontal transport.

3.4. Factors Controlling the $CaCO_3$ and Opal Export

[43] We investigate the possible factors controlling the export of $CaCO_3$ and opal on the basis of a correlation and multiple linear regression analysis. We use the correlation analysis to identify first those variables that have potentially predictive power, and then employ a step-wise multiple linear regression analysis to develop a predictive model of opal and $CaCO_3$ export. We limit our analysis here to the standard results from the P2A model.

[44] We investigated a total of 17 independent variables, all taken from the diagnostic model. These variables can be grouped into three categories: (1) general environmental conditions, (2) production terms, and (3) limitation terms. The variables considered in the first group are sea surface temperature (SST), salinity (SAL), concentrations of PO_4, NO_3, silicic acid ($Si(OH)_4$), and potential alkalinity (PAlk). The second group includes chlorophyll, NPP, large phytoplankton production (NPP_L), small phytoplankton production (NPP_S), export of POC (Φ_{POC}), export of organic carbon (Φ_{Corg}), export of opal (Φ_{SiO_2}), and export of $CaCO_3$ (Φ_{POC}). Although chlorophyll is not explicitly modeled, we can estimate it from NPP assuming a constant Chl:N ratio,

	Zonal	$10°\times10°$	ICE	SP	ST–SS	ST–PS	LL–U	Eq–U	Eq–D
S	(−8)	(−2)	44	13	−47	−15	−12	−17	(−41)
T	−56	−40	15	−24	−48	−46	−28	−78	(37)
PO_4	94	74	64	66	60	64	68	87	66
NO_3	97	76	62	68	57	76	61	87	53
$Si(OH)_4$	90	79	77	66	65	68	69	85	72
PAlk	86	48	64	61	63	56	47	60	(28)
NPP	(7)	30	80	52	50	49	83	81	58
NPP_L	(43)	48	80	59	57	68	89	83	55
NPP_S	(−17)	11	79	40	39	31	73	77	59
Chl	82	74	80	72	67	79	86	85	53
Φ_{CaCO3}	(46)	42	74	25	43	63	70	70	51
Φ_{POC}	78	70	81	68	68	79	88	86	55
Φ_{Corg}	70	63	76	66	60	65	79	82	(0)
$\Delta N/\Delta t$	(39)	44	82	12	46	33	49	62	(26)
Z_m	89	76	88	32	41	−12	−15	−26	(−22)
ΔZ_{mld}	97	70	71	61	42	79	−20	−51	(−43)
E_{cr}	(−29)	−26	27	35	−31	−18	−25	−35	(26)

Figure 6. Same as Figure 5 except for opal export.

i.e., $Chl = 1/\mu_0 \cdot e^{-kT} \cdot \frac{Chl}{N}$ NPP, where μ_0, is the growth rate and k is the temperature dependence of phytoplankton growth (see auxiliary Table S1). The last group includes the monthly variations in nitrate ($\Delta N/\Delta t$), the critical irradiance parameter (E_{cr}), mixed layer depth (Z_m) and the stability depth (ΔZ_{mld}), which have been found useful in determining the monthly probability distributions of coccolithophorids [*Iglesias-Rodriguez et al.*, 2002b] (see auxiliary Table S3 in supplementary material for definitions).

[45] Before determining the correlations, we aggregated the data to larger regions in order to avoid the considerable uncertainties associated with the fluxes at the grid point level. We used two different levels of aggregation. In the first aggregation, we combined all grid cells to $10° \times 10°$ regional tiles. In the next level, we further aggregated the results into $10°$ zonal bands. We also tested an alternative approach, where the analysis was done on a grid cell base level, but separately for seven different biomes, as defined by the criteria proposed by *Sarmiento et al.* [2004b] (see auxiliary Table S2).

[46] The correlation coefficients between the variables and $CaCO_3$ export are shown in Figure 5. Variables of the production category, for example, chlorophyll, and primary and export production have high correlation coefficients with $CaCO_3$ export. This is a direct reflection of the rain ratio being relatively uniform, requiring that the $CaCO_3$ export correlates strongly with export production. The same argument applies to most nutrients, which also show substantial positive correlations. Confirming *Iglesias-Rodriguez et al.* [2002b], the monthly N drawdown, $\Delta N/\Delta t$, and the mixed layer depth, Z_m, have some predictive power for $CaCO_3$ export as well.

[47] The remaining variables have little or regionally strongly differing correlations with $CaCO_3$ export. Temperature has a significant negative correlation in several bio-

mes. The level of temperature fluctuation has also been considered as a major factor in distinguishing coccolithophorids bloom regions [*Iglesias-Rodriguez et al.*, 2002b] or regions with elevated $CaCO_3$ production [*Moore et al.*, 2002]. However, given the strong anticorrelation of SST with nutrients, it is unclear whether this negative correlation with SST is due to growth effects or due to nutrient availability.

[48] Similar to the export of $CaCO_3$, the correlations between opal export and the independent variables of the production category are quite strong, except for the $10°$ zonal band aggregation in which NPP, NPP_L, and NPP_S are not significant at the 95% significance level using a t-test (Figure 6). Nutrients also emerge as an important predictor for opal export, particularly $Si(OH)_4$. This is consistent with our view that diatoms tend to outcompete other phytoplankton in the presence of $Si(OH)_4$. The mixed layer depth, Z_m, and the stability depth, ΔZ_{mld}, have high positive correlations in most extratropical regions, but have little predictive power in the tropics. In some cases, the correlations are even negative. The critical irradiance exhibits small to moderate negative correlations.

[49] On the basis of these correlations, we developed empirical models that predict the export of opal and $CaCO_3$ as a linear combination of the most important predictor variables. For each of the three aggregations, i.e., $10°$ zonal, $10° \times 10°$, and regional biomes, we used a step-wise linear regression analysis, where all linear combinations of independent variables were tested until a combination was found that yielded the highest regression coefficient and the smallest residual, but had not more than three independent variables.

[50] For zonal and the $10° \times 10°$ aggregations, the best predictions of $CaCO_3$ export are found when NPP, $Si(OH)_4$, and PO_4 are used as independent variables (see auxiliary

Table S3). At first glance, it is surprising that $Si(OH)_4$ turns out to be a good predictor variable for $CaCO_3$ export, while its correlation is not particularly high (see Figure 5). The reason is that many variables that have high correlations with $CaCO_3$ export have high correlations with each other, so that the addition of a variable with a weaker correlation with $CaCO_3$ export can improve the quality of the fit more than the addition of a variable with higher correlation with $CaCO_3$ export, but one that has a strong correlation with the already employed independent variables. The global mean errors for the two levels of aggregation are similar, although the r^2 for the zonal aggregation, 0.88, is much larger than that for the $10° \times 10°$ aggregation, 0.41. This is a direct consequence of the much smaller number of degrees of freedom in the former case (17 instead of 562). Dividing the whole ocean into biomes gives similar results with a relatively small reduction of the error (auxiliary Table S3). This is primarily because $CaCO_3$ export is a relatively constant fraction of NPP, irrespective of the region considered.

[51] As is the case for the export of $CaCO_3$, the export of opal can be estimated by using just three independent variables, i.e., $Si(OH)_4$, chlorophyll, and ΔZ_{mld}. Although the empirical equation for the zonal mean captures the zonal mean features well, it fails to produce the high opal export in the eastern tropical Pacific and the northern North Pacific, which represent key features in the diagnosed opal export and in observations. The empirical equation for the $10° \times 10°$ aggregation improves this substantially. As found for $CaCO_3$ export, dividing the whole ocean into biomes gives similar results (auxiliary Table S3).

[52] Therefore we suggest using the empirical equations from the $10° \times 10°$ aggregation to predict $CaCO_3$ and opal export,

$$\Phi_{CaCO_3} = \max(0, -0.08 + 0.016 \cdot NPP + 0.0037 \cdot Si(OH)_4), \tag{2}$$

$$\Phi_{SiO_2} = \max\left(0, -0.35 + 0.030 \cdot Si(OH)_4 + 0.17 \cdot Chl\right), \tag{3}$$

where Φ_{CaCO_3}, Φ_{SiO_2}, and NPP are given in units of mol m^{-2} yr^{-1}, $Si(OH)_4$ in mmol m^{-3}, and Chl in mg Chl m^{-3}. The mean absolute error of these two equations are 0.17 and 0.33 mol m^{-2} yr^{-1} respectively, primarily driven by the inability of these aggregated equations to accurately represent the maxima in $CaCO_3$ and opal export in Figure 2. The auxiliary material provides empirical equations for these two fluxes that use just physical properties as independent variables (auxiliary Table S4).

4. Phytoplankton Functional Groups and Their Contribution to NPP and POC Export

[53] Next, we use our diagnosed export fluxes of $CaCO_3$ and opal and combine them with the organic carbon export estimates derived from the BGC-model to arrive at an estimate of the relative contribution of coccolithophorids and diatoms to export production. This requires estimates of the stoichiometric ratios of organic carbon to $CaCO_3$ for the coccolithophorids and for the ratio of organic carbon to opal for the diatoms. If we further add an estimate of the fraction of $CaCO_3$ and opal that dissolves in the euphotic zone before they are exported, we can finally estimate the relative contribution of coccolithophorids and diatoms to NPP, which together with the model-based allocation of NPP to small and large phytoplankton yields a complete description of the relative contribution to NPP of all major phytoplankton functional groups we consider. We then discuss these results in the context of an allocation tree, which asks, given a certain amount of NPP, which functional groups are responsible for it? This decision tree will be the basis for the semiprognostic model we aim to develop in the future.

[54] In the following analyses, we make the assumption that all of the opal export is driven by diatoms and all of the $CaCO_3$ export is driven by coccolithophorids. Given these assumptions our estimates for coccolithophorids and opal are upper limit estimates. Globally, we suspect that the neglect of foraminifera and pteropods will lead to a reasonably small error, but this is quite certainly not the case at the regional level. Pteropods, for example, have been shown to dominate the export of $CaCO_3$ in the Ross Sea [*Collier et al.*, 2000]. Furthermore, foraminifera have been found to contribute up to 60% of the $CaCO_3$ flux to depth in the Arabian Sea [*Iglesias-Rodriguez et al.*, 2002a]. This caveat needs to be considered when analyzing the results.

4.1. Methods

[55] The estimation of the export of organic carbon driven by diatoms and coccolithophorids, i.e., Φ_{Corg}^{diatom} and Φ_{Corg}^{cocco}, requires an estimate of the silicon to organic carbon ratio, $r_{SiO_2:C_{org}}$, of diatoms, and of the inorganic to organic carbon ratio, $r_{CaCO_3:C_{org}}$, of coccolithophorids, thus

$$\Phi_{C_{org}}^{diatom} = \frac{\Phi_{SiO_2}}{r_{SiO_2:C_{org}}} \tag{4}$$

$$\Phi_{C_{org}}^{cocco} = \frac{\Phi_{CaCO_3}}{r_{CaCO_3:C_{org}}}. \tag{5}$$

[56] The $CaCO_3$ to organic carbon ratio in coccolithophorids is not known well. As reviewed by *Paasche* [2002], reported $C_{CaCO_3}:C_{org}$ ratios vary from 0.40 to 2.30. Low irradiance [*Paasche*, 1999] and low temperatures [*Paasche*, 2002] during growth tend to decrease the $C_{CaCO_3}:C_{org}$ ratio, while nutrient limitation tends to increase it [*Paasche*, 1998]. Despite this complexity, it turns out that on average, the $C_{CaCO_3}:C_{org}$ ratio of coccolithophorids is about 1:1. We adopt this ratio here, but need to consider that uncertainties in this ratio propagate directly to our results.

[57] The silicon to nitrogen ratio of diatoms grown under nutrient replete conditions is around 1:1, albeit with some variations from species to species [*Brzezinski*, 1985]. Much larger variations in this ratio are caused by silicic acid and iron limitation. Iron limitation has been demonstrated to increase the Si:N ratio to values as large 3:1 in coastal areas and several HNLC regions including the subarctic Pacific,

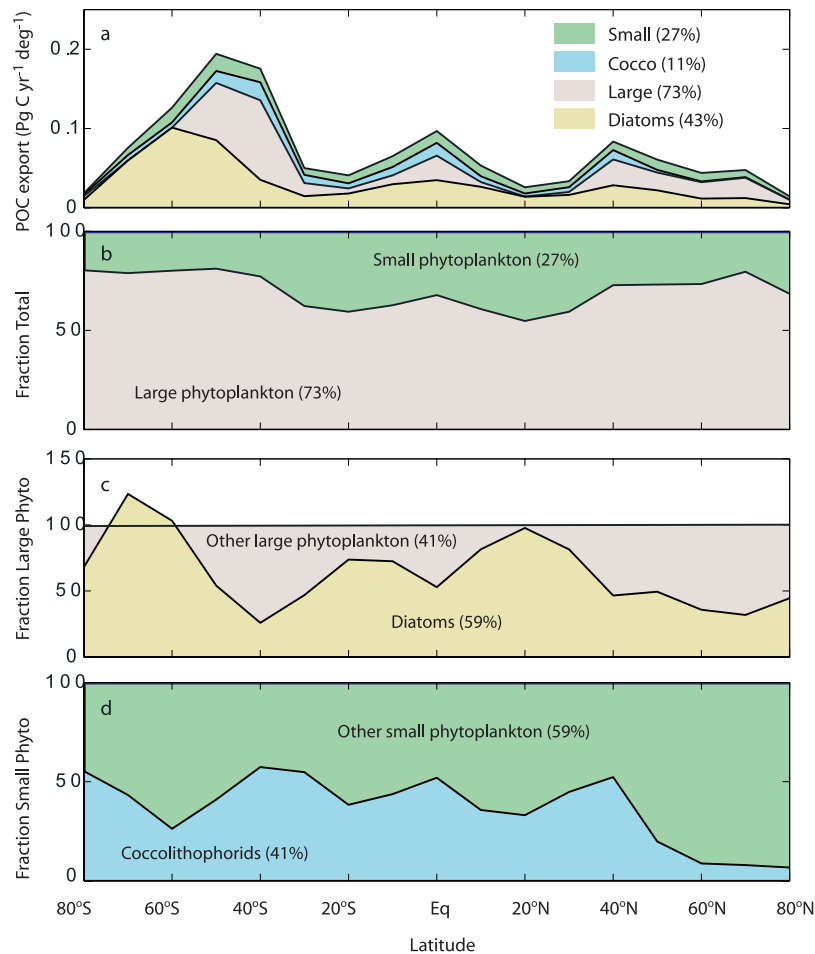**Table 3.** Global Contribution of the Functional Groups to NPP and POC Export

	NPP[a]			Φ_{POC}[a]			Φ_{POC}/NPP		
	P2A(std)	HH	LL	P2A(std)	HH	LL	P2A(std)	HH	LL
Large phytoplankton	0.31(23.8)	0.32(30.8)	0.30(21.9)	0.73(7.2)	0.73(8.3)	0.71(6.1)	0.30	0.27	0.28
Small phytoplankton	0.69(54.2)	0.68(65.2)	0.70(51.1)	0.27(2.6)	0.27(3.0)	0.29(2.5)	0.05	0.05	0.05
Diatoms	0.14(10.7)	0.13(12.6)	0.12(9.1)	0.43(4.2)	0.39(4.4)	0.36(3.1)	0.40	0.35	0.34
Coccolithophorids	0.01(1.1)	0.01(1.2)	0.01(1.0)	0.11(1.1)	0.10(1.1)	0.12(1.0)	0.98	0.99	0.99

[a]Numbers represent fractional contribution to total, while the numbers in parentheses are the corresponding absolute values in units of PgC yr^{-1}.

equatorial Pacific and Southern oceans [*Hutchins and Bruland*, 1998; *Takeda*, 1998]. Ratios as high as 5:1 have been reported from the Southern Ocean [*Franck et al.*, 2000; *Brzezinski et al.*, 2003], consistent with iron limitation playing a crucial role. To capture the main features of these variations, we estimate the Si:N ratio of diatoms using a simplified model of diatom physiology taking into consideration the limitation by silicic acid, iron, and other factors (see auxiliary material and J. Dunne et al., Ecology and biogeochemistry in a 43-year ice/ocean reanalysis in a

global ocean biogeochemical general circulation model, manuscript in preparation, 2006) for details). The resulting Si:N ratio of diatoms varies between 4:1 in the Southern Ocean and about 0.5 to 2:1 throughout the rest of the ocean, except for the North Pacific, where this ratio increases up to 4:1 (see auxiliary Figure S1a). The Si to organic carbon ratio, $r_{SiO_2:C_{org}}$, is finally calculated from the Si:N ratio using a fixed C:N ratio of 117:16.

[58] Finally, in order to obtain the contribution of the diatoms and coccolithophorids to NPP, i.e., P_{diatom} and

Figure 7. Zonal mean POC export by the different phytoplankton functional groups and fractional contributions. (a) Zonal integrals of the POC export driven by the four different phytoplankton functional groups considered. (b) Fraction of POC export driven by large and small phytoplankton. (c) Fraction of large phytoplankton POC export driven by diatoms. (d) Fraction of small phytoplankton POC export driven by coccolithophorids.
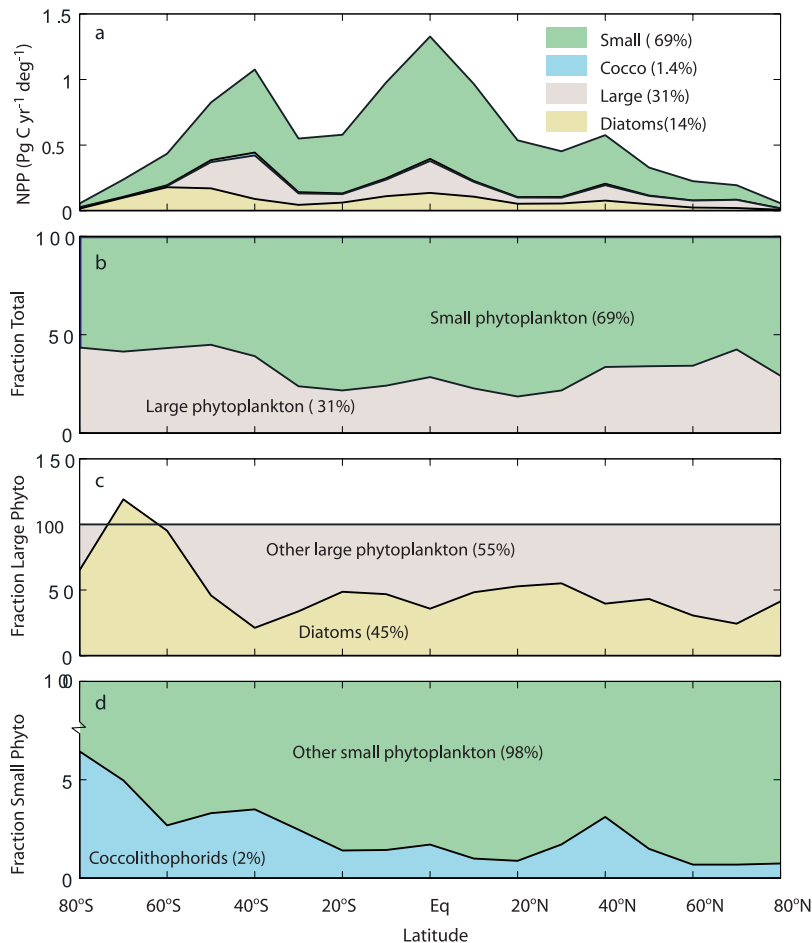
Figure 8. Same as Figure 7 except for NPP.

P_{cocco}, we need to estimate the fraction of opal and $CaCO_3$ that gets dissolved in the euphotic zone, i.e., γ_{diss}^{diatom} and γ_{diss}^{cocco},

$$P_{diatom} = \left(1 - \gamma_{diss}^{diatom}\right)^{-1} \cdot \Phi_{C_{org}}^{diatom} \qquad (6)$$

$$P_{cocco} = \left(1 - \gamma_{diss}^{cocco}\right)^{-1} \cdot \Phi_{C_{org}}^{cocco}. \qquad (7)$$

[59] We estimate the opal fraction, γ_{diss}^{diatom}, dissolving in the euphotic zone on the basis of a temperature dependent opal dissolution model [Hurd and Birdwhistell, 1983] (see auxiliary material). The inferred global mean fraction is about 0.5, consistent with the global estimates of Nelson et al. [1995] and Ragueneau et al. [2002]. Spatially, the ratio γ_{diss}^{diatom} varies between about 0.3 in the high latitudes, and about 0.7 in the low latitudes (see auxiliary Figure S1b). For $CaCO_3$, we assume that no dissolution occurs in the euphotic zone, i.e., $\gamma_{diss}^{cocco} = 0$, on the basis of the argument that surface waters are supersaturated with respect to $CaCO_3$. However, there is evidence of $CaCO_3$ dissolution above the aragonite and calcite saturation horizons

[Milliman et al., 1999]. If this result extended into the euphotic zone, our estimated contribution of coccolitho-phorids to NPP would be an underestimate.

4.2. Functional Groups and POC Export

[60] The contribution of the different functional groups considered in our study to the export of POC varies considerably (Table 3 and Figure 7). In our standard model, P2A, large phytoplankton dominate POC export with 73% of POC export associated with this functional group. The remaining 27% is associated with small phytoplankton. Diatoms and coccolithophorids account for about 40% and about 10% of total POC export, respectively. These percentages are remarkably insensitive to which OGCM is employed, as they vary by only a few percentage points when HH or LL are used (Table 3). We therefore limit our further discussion to the standard case. We also do not consider the negative restoring term case here (P2A-neg), because the consideration of negative production is in conflict with the way the ecosystem model is constructed.

[61] The dominance of large phytoplankton is particularly strong in the high latitudes, and especially so in the Southern Ocean, where they are driving about 80% of POC export. In the low latitudes, their contribution shrinks

to about 55% (Figure 7b). Diatoms are responsible for the majority of large phytoplankton export with a global fraction of about 60% (Figure 7c). In the Southern Ocean and in the tropics, almost all large phytoplankton export comes from diatoms. Other large phytoplankton make a substantial contribution only around 40°S and 60°N. Since the export of opal and organic carbon are diagnosed independently of each other and are subject to their own uncertainties and biases, the diatom export fraction can be larger than 100%, as is the case in the Southern Ocean. We have not made any attempt to force this ratio to be smaller than one. Therefore the offset can be viewed as an estimate of the uncertainty in our model diagnosed estimates.

[62] Somewhat less than half of the export driven by small phytoplankton comes from coccolithophorids (Figure 7d). The relative fraction is fairly constant except north of 40°N where it decreases to about 5%. This diagnosed result provides some confirmation that the assumption made in several modeling studies that $CaCO_3$ export represents a fixed fraction of nondiatom production export may be reasonable [*Archer et al.*, 2000; *Matsumoto et al.*, 2002]. The ratio of $CaCO_3$ export to nondiatom production export amounts to about 20% in our results, with variations of less than 10% south of 40°N. North of this latitude, this ratio decreases to 3%.

[63] The particle export ratios for these different phytoplankton functional groups are also listed in Table 3. We refer to Dunne et al. (manuscript in preparation, 2006) for their discussion.

4.3. Functional Groups and NPP

[64] The contribution of the different functional groups to NPP (Table 3 and Figure 8) is very different from that to POC export. Small phytoplankton dominate NPP, being responsible for nearly 70% of it. Large phytoplankton production accounts for about 30%, while diatoms and coccolithophorids account for about 15% and less than 2%, respectively. As was the case for export, these percentages vary little among the three employed OGCMs (Table 3). We therefore also limit our further discussion to the standard case.

[65] In general, NPP driven by the different functional groups exhibit similar latitudinal variations with elevated values in the high latitudes and the equator, and low values in the subtropical gyres (Figure 8a). The latitudinal distribution of the relative fractions of small to large phytoplankton in NPP is similar to that of POC export, except for a constant offset (compare Figure 8b with 7b). This offset reflects primarily the much higher fraction of small phytoplankton biomass being recycled in the euphotic zone before it is exported.

[66] Among large phytoplankton, the contribution of diatoms to NPP is globally about 45%. As expected, diatoms tend to dominate in the Southern Ocean, where they are responsible for almost all of the large phytoplankton NPP (Figure 8c). Elsewhere, diatoms are found to drive about half of large phytoplankton NPP.

[67] Coccolithophorids account for only a small fraction of small phytoplankton NPP with a global mean of 2%. The

meridional distribution of their fraction is relatively uniform (Figure 8d).

[68] A comparison of our NPP contribution estimates with a HPLC pigment based summary of the relative abundances of these phytoplankton functional groups by *Gregg et al.* [2003] shows reasonable agreement for diatoms (see auxiliary Table S5). However, our diagnosed relative contribution of coccolithophorids to NPP is much smaller than the relative abundance estimated from the pigment data, for reasons not entirely clear (see auxiliary material for an in-depth discussion).

4.4. Allocation Tree of NPP

[69] We summarize our results in an allocation tree, which describes how NPP is allocated to the different phytoplankton functional groups considered (Figure 9). The first allocation can be thought to occur between small and large phytoplankton. Our model finds that this occurs with a ratio of 0.69:0.31. In our model, the factors that determine this ratio are nutrient availability and grazing, with the small phytoplankton being subject to much stronger grazing control than the large phytoplankton. We expect these factors also to be the dominant ones in the real ocean. At the next level, the factor $\Omega_{NPP_S}^{cocco}$ determines how NPP is allocated to coccolithophorids within the small phytoplankton, and $\Omega_{NPP_L}^{diatom}$ describes how NPP is allocated to diatoms within the large phytoplankton. Our model diagnoses that diatoms account for 45% of large phytoplankton, in agreement with the assumption that diatoms tend to outcompete most other phytoplankton. Coccolithophorids account for only 2% of small phytoplankton NPP, and about 1.5% of total phytoplankton NPP. The factors that determine these allocations are not well known, but will be determined and discussed in the next subsection.

[70] The different functional groups exhibit also rather different ratios of POC export to NPP, called pe-ratios [*Dunne et al.*, 2005]. As expected, diatoms have high pe-ratios (0.40), and account for a large fraction of the POC export (0.43). On the basis of our assumptions of no dissolution of $CaCO_3$ in the euphotic zone and a $CaCO_3:C_{org}$ ratio of 1:1, coccolithophorids have a pe-ratio of 1. This leads them to contribute around 10% to global POC export despite the fact that they account for only less than 2% of global NPP. In contrast, the pe-ratio of noncalcifying small phytoplankton is only 0.03, so that their contribution to global POC export is also around 10%, despite the fact that this functional group is responsible for nearly 70% of global NPP.

4.5. Empirical Equations for Ratios $\Omega_{NPP_S}^{cocco}$ and $\Omega_{NPP_L}^{diatom}$

[71] In order to determine which environmental factors may control the allocation ratios $\Omega_{NPP_S}^{cocco}$ and $\Omega_{NPP_L}^{diatom}$ (Figure 9), we performed a correlation and stepwise multiple linear regression analysis similar to that undertaken for Φ_{CaCO_3} and Φ_{SiO_2}. The correlation analyses reveal for $\Omega_{NPP_S}^{cocco}$ significant correlations for nearly all variables, with the highest values for the nutrients and variables associated with the vertical stability, i.e., mixed layer depth (Z_m) and the stability depth (ΔZ_{mld}) (see auxiliary Figure S2). Inter-
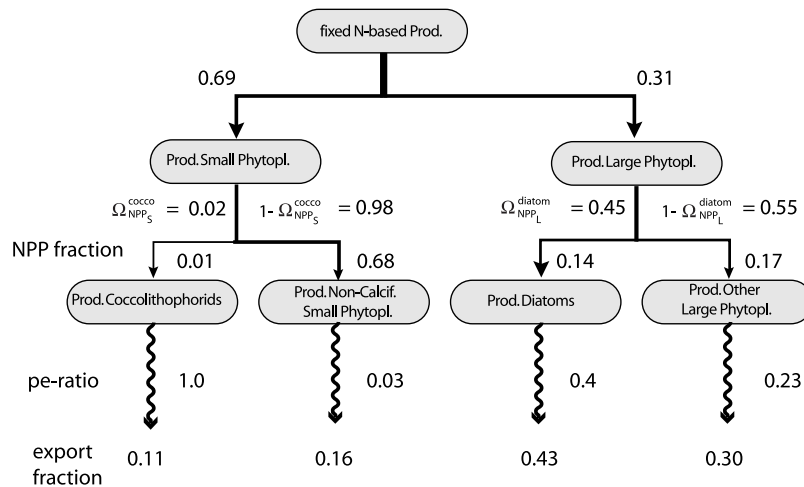
Figure 9. Global allocation of NPP to the four functional groups considered in this study. The numbers shown at the bifurcation points are fractions. Also shown are the pe ratios (ratios of POC export to NPP [*Dunne et al.*, 2005]) and the export fraction associated with each phytoplankton function group.

estingly, the same variables also show high correlations with $\Omega_{NPP_L}^{diatom}$. Auxiliary Table S6 shows the best linear regression equations for the global as well as for the regional aggregations. Our global results for the $10° \times 10°$ aggregation suggests the following empirical relationships:

$$\Omega_{NPP_S}^{cocco} = \max\left(0, 0.0027 + 0.00057 \cdot \text{Si(OH)}_4 + 0.00083 \cdot NPP_S\right) \tag{8}$$

$$\Omega_{NPP_L}^{diatom} = \max\left(0, 0.60 + 0.014 \cdot \text{Si(OH)}_4 - 0.065 \cdot Chl\right), \tag{9}$$

where Si(OH)_4 and NO_3 are given in units of mmol m^{-3}, NPP_S in units of mol m^{-2} yr^{-1}, and Chl in units of mg Chl m^{-3}. The online supplementary material shows also empirical equations for these two allocation ratios that use just physical properties as independent variables (auxiliary Table S7).

[72] These results are surprising at first glance, as the finding of a predictive power of silicic acid for both ratios appears to contradict the idea that increased silicic acid concentration would lead to greater diatom production and consequently to a lesser abundance of coccolithophorids [e.g., *Archer et al.*, 2000; *Matsumoto et al.*, 2002; *Harrison*, 2000; *Brzezinski et al.*, 2002]. However, before one draws such a conclusion, one needs to consider that the two ratios are expressed relative to small and large phytoplankton NPP and not to total NPP. Expressed in terms of total NPP, the fraction of diatoms versus coccolithophorids is

$$\frac{P_{diatom}}{P_{cocco}} = \frac{\Omega_{NPP_L}^{diatom} \cdot \Omega_{NPP}^{L}}{\Omega_{NPP_S}^{cocco} \cdot \left(1 - \Omega_{NPP}^{L}\right)}, \tag{10}$$

where Ω_{NPP}^{L} is the fraction of large phytoplankton to NPP. It turns out that the ratio Ω_{NPP}^{L} is also strongly positively

correlated with the silicic acid concentration, and with a regression coefficient of 0.00316 that is larger than that associated with $\Omega_{NPP_S}^{cocco}$ in (8). As a result, the enumerator in (10) increases much more strongly with increased silicic acid concentrations than the denominator, causing the relative fraction to NPP of diatoms versus that of coccolithophorids to scale positively with the silicic acid concentration as well. Thus our findings confirm the idea that higher silicic acid concentrations lead to a higher diatom productivity at the cost of coccolithophorids, as proposed to have occurred during the last glacial [e.g., *Archer et al.*, 2000; *Matsumoto et al.*, 2002].

5. Outlook

[73] Given the lack of quantitative information about functional groups and their associated export of organic matter and biogenic minerals, our results can provide one of the few means to evaluate prognostic models of phytoplankton functional groups such as those of *Moore et al.* [2004] and *Gregg et al.* [2003]. This requires a good understanding of the uncertainties associated with our results. While many of our conclusions turn out to be remarkably robust within the bounds of the investigated assumptions, data and models, our consideration of biases is by no means exhaustive. In particular, models run at much higher resolutions, or with very different grids and forcing may yield results that lie outside our bounds. However, experience from model intercomparison studies [e.g., *Doney et al.*, 2004; *Matsumoto et al.*, 2004; *Mikaloff-Fletcher et al.*, 2006] indicate that the three models used here span a large range of possible model behavior.

[74] We next plan to use our results to develop a semi-prognostic model that combines the allometric model of Dunne et al. (manuscript in preparation, 2006) with our empirical allocation factors to predict phytoplankton production and diversity in a changing world. Our empirical allocation factors can also be combined with the empirical

chlorophyll equations of *Sarmiento et al.* [2004b] to estimate phytoplankton abundance and diversity for a large suite of climate models to which no biological/biogeochemical model has been coupled yet.

References

Archer, D. E., A. Winguth, D. Lea, and N. Mahowald (2000), What caused the glacial/interglacial atmospheric pCO₂ cycles?, *Rev. Geophys.*, *38*(2), 159–189.

Armstrong, R. A., C. Lee, J. I. Hedges, S. Honjo, and S. G. Wakeham (2002), A new, mechanistic model for organic carbon fluxes in the ocean based on the quantitative association of POC with ballast minerals, *Deep Sea Res., Part II*, *49*, 219–236.

Balch, W. M., H. R. Gordon, B. C. Bowler, D. T. Drapeau, and E. S. Booth (2005), Calcium carbonate measurements in the surface global ocean based on moderate-resolution imaging spectroradiometer data, *J. Geophys. Res.*, *110*, C07001, doi:10.1029/2004JC002560.

Bates, N. R., A. F. Michaels, and A. H. Knap (1996a), Seasonal and inter-annual variability of oceanic carbon dioxide species at the U.S. JGOFS Bermuda Atlantic Time-series Study (BATS) site, *Deep Sea Res., Part II*, *43*, 347–383.

Bates, N. R., A. F. Michaels, and A. H. Knap (1996b), Alkalinity changes in the Sargasso Sea: Geochemical evidence of calcification?, *Mar. Chem.*, *51*, 347–358.

Brewer, P., G. Wong, M. Bacon, and D. Spencer (1975), An oceanic calcium problem?, *Earth Planet. Sci. Lett.*, *26*, 81–87.

Brown, C. W., and J. A. Yoder (1994), Coccolithophorid blooms in the global ocean, *J. Geophys. Res.*, *99*, 7467–7482.

Brzezinski, M. (1985), The Si:C:N ratio of marine diatoms: Interspecific variability and the effect of some environmental variables, *J. Phycol.*, *21*, 347–357.

Brzezinski, M. A., J. L. Sarmiento, K. Matsumoto, C. J. Pride, D. M. Sigman, N. Gruber, G. H. Rau, and K. H. Coale (2002), A switch from Si(OH)₄ to NO₃⁻ depletion in the glacial Southern Ocean, *Geophys. Res. Lett.*, *29*(12), 1564, doi:10.1029/2001GL014349.

Brzezinski, M. A., M.-L. Dickson, D. Nelson, and R. Sambrotto (2003), Ratios of Si, C and N uptake by microplankton in the Southern Ocean, *Deep Sea Res., Part II*, *50*, 619–633.

Buesseler, K. O., L. Ball, J. Andrews, C. Benitez-Nelson, R. Belastock, F. Chai, and Y. Chao (1998), Upper ocean export of particulate organic carbon in the Arabian Sea derived from Thorium-234, *Deep Sea Res., Part II*, *45*, 2461–2487.

Capone, D. G., J. A. Burns, J. P. Montoya, A. Subramaniam, C. Mahaffey, T. Gunderson, A. F. Michaels, and E. J. Carpenter (2005), Nitrogen fixation by *Trichodesmium* spp.: An important source of new nitrogen to the tropical and subtropical North Atlantic Ocean, *Global Biogeochem. Cycles*, *19*, GB2024, doi:10.1029/2004GB002331.

Collier, R., J. Dymond, S. Honjo, S. Manganini, R. Francois, and R. Dunbar (2000), The vertical flux of biogenic and lithogenic material in the Ross Sea: Moored sediment trap observations 1996–1998, *Deep Sea Res., Part II*, *47*, 3491–3520.

Conkright, M. E., R. A. Locarnini, H. Garcia, T. O. Brien, T. Boyer, C. Stephens, and J. Antonov (2002), *World Ocean Atlas 2001: Objective Analyses, Data Statistics, and Figures CD-ROM Documentation* [CD-ROM], *WOA01*, Natl. Oceanogr. Data Cent., Silver Spring, Md.

Doney, S. C., et al. (2004), Evaluating global ocean carbon models: The importance of realistic physics, *Global Biogeochem. Cycles*, *18*, GB3017, doi:10.1029/2003GB002150.

Dunne, J., R. A. Armstrong, A. Gnanadesikan, J. L. Sarmiento, and R. D. Slater (2005), Empirical and mechanistic models for particle export ratio, *Global Biogeochem. Cycles*, *19*, GB4026, doi:10.1029/2004GB002390.

Feely, R. A., C. L. Sabine, K. Lee, W. Berelson, J. Kleypas, V. J. Fabry, and F. J. Millero (2004), Impact of anthropogenic CO₂ on the CaCO₃ system in the oceans, *Science*, *305*, 362–366.

Franck, V. M., M. A. Brzezinski, K. H. Coale, and D. M. Nelson (2000), Iron and silicic acid concentrations regulate Si uptake north and south of the Polar Frontal Zone in the Pacific sector of the Southern Ocean, *Deep Sea Res., Part II*, *47*, 3315–3338.

Friis, K., A. Kortzinger, and D. Wallace (2003), The salinity normalization of marine inorganic carbon chemistry data, *Geophys. Res. Lett.*, *30*(2), 1085, doi:10.1029/2002GL015898.

Gibb, S., R. Barlow, D. Cummings, N. Rees, C. Trees, P. Holligan, and D. Suggett (2000), Surface phytoplankton pigment distributions in the Atlantic Ocean: An assessment of basin scale variability between 50°N and 50°S, *Prog. Oceanogr.*, *45*, 339–368.

Gnanadesikan, A. (1999), A global model of silicon cycling: Sensitivity to eddy parameterizations and dissolution, *Global Biogeochem. Cycles*, *13*(1), 199–220.

Gnanadesikan, A., N. Gruber, R. D. Slater, and J. L. Sarmiento (2002), Oceanic vertical exchange and new production: A comparison between model results and observations, *Deep Sea Res., Part II*, *49*, 363–401.

Gnanadesikan, A., J. P. Dunne, R. M. Key, K. Matsumoto, J. L. Sarmiento, R. D. Slater, and P. S. Swathi (2004), Oceanic ventilation and biogeochemical cycling: Understanding the physical mechanisms that produce realistic distributions of tracers and productivity, *Global Biogeochem. Cycles*, *18*, GB4010, doi:10.1029/2003GB002097.

Gordon, H. R., G. C. Boynton, W. M. Balch, S. B. Groom, D. S. Harbour, and T. J. Smyth (2001), Retrieval of coccolithophore calcite concentration from SeaWiFS imagery, *Geophys. Res. Lett.*, *28*(8), 1587–1590.

Gregg, W. W., P. Ginoux, P. S. Schopf, and N. W. Casey (2003), Phytoplankton and iron: Validation of a global three-dimensional ocean biogeochemical model, *Deep Sea Res., Part II*, *50*, 3143–3169.

Gruber, N. (2004), The dynamics of the marine nitrogen cycle and atmospheric CO₂, in *Carbon Climate Interactions*, edited by T. Oguz and M. Follows, pp. 97–148, Springer, New York.

Gruber, N., and J. L. Sarmiento (1997), Global patterns of marine nitrogen fixation and denitrification, *Global Biogeochem. Cycles*, *11*(2), 235–266.

Harrison, K. G. (2000), Role of increased marine silica input on paleo-pCO₂ levels, *Paleoceanography*, *15*(3), 292–298.

Heinze, C., A. Hupe, and E. Maier-Reimer (2003), Sensitivity of the marine biospheric Si cycle for biogeochemical parameter variations, *Global Biogeochem. Cycles*, *17*(3), 1086, doi:10.1029/2002GB001943.

Honjo, S., R. Francois, S. Manganini, J. Dymond, and R. Collier (2000), Particle fluxes to the interior of the Southern Ocean in the Western Pacific sector along 170°W, *Deep Sea Res., Part II*, *47*, 3521–3548.

Honjo, S., R. Francois, R. Krishfield, and S. Manganini (2003), Global export flux and regional functionality of biological pump: A result from JGOFS sediment trap programs since 1982, *Rep. 38*, p. 46, Joint Global Ocean Flux Study, Bergen, Norway.

Hurd, D., and S. Birdwhistell (1983), On producing a general model for biogenic silica dissolution, *Am. J. Sci.*, *283*, 1–28.

Hutchins, D. A., and K. W. Bruland (1998), Iron-limited diatom growth and Si:N uptake ratios in a coastal upwelling regime, *Nature*, *393*, 561–564.

Hutchinson, G. (1961), The paradox of the plankton, *Am. Nat.*, *95*, 137–145.

Iglesias-Rodriguez, M. D., R. Armstrong, R. A. Feely, R. Hood, J. Kleypas, J. D. Milliman, C. S. Sabine, and J. L. Sarmiento (2002a), Progress made in study of ocean's carbonate budget, *Eos Trans. AGU*, *83*(34), 365, 374–375.

Iglesias-Rodriguez, M. D., C. W. Brown, S. C. Doney, J. A. Kleypas, D. Kolber, Z. Kolber, P. Hayes, and P. G. Falkowski (2002b), Representing key phytoplankton functional groups in ocean carbon cycle models: Coccolithophorids, *Global Biogeochem. Cycles*, *16*(4), 1100, doi:10.1029/2001GB001454.

Karl, D. M., et al. (2002), Dinitrogen fixation in the world's ocean, *Biogeochemistry*, *57/58*, 47–98.

Keeling, C., H. Brix, and N. Gruber (2004), Seasonal and long-term dynamics of the upper ocean carbon cycle at station ALOHA near Hawaii, *Global Biogeochem. Cycles*, *18*, GB4006, doi:10.1029/2004GB002227.

Key, R., et al. (2004), A global ocean carbon climatology: Results from Global Data Analysis Project (GLODAP), *Global Biogeochem. Cycles*, *18*(4), GB4031, doi:10.1029/2004GB002247.

Klaas, C., and D. E. Archer (2002), Association of sinking organic matter with various types of mineral ballast in the deep sea: Implications for the rain ratio, *Global Biogeochem. Cycles*, *16*(4), 1116, doi:10.1029/2001GB001765.

Lamb, M. F., et al. (2002), Consistency and synthesis of Pacific Ocean CO₂ survey data, *Deep Sea Res., Part II*, *49*, 21–58.

Lee, K. (2001), Global net community production estimated from the annual cycle of surface water total dissolved inorganic carbon, *Limnol. Oceanogr.*, *46*(6), 1287–1297.

Li, Y. H., T. Takahashi, and W. S. Brecker (1969), Degree of saturation of CaCO₃ in the oceans, *J. Geophys. Res.*, *74*, 5507–5525.

Matsumoto, K., J. L. Sarmiento, and M. A. Brzezinski (2002), Silicic acid leakage from the Southern Ocean as possible mechanism for explaining glacial atmospheric pCO₂, *Global Biogeochem. Cycles*, *16*(3), 1031, doi:10.1029/2001GB001442.

Matsumoto, K., et al. (2004), Evaluation of ocean carbon cycle models with data-based metrics, *Geophys. Res. Lett.*, *31*, L07303, doi:10.1029/2003GL018970.

Mikaloff-Fletcher, S. E., et al. (2006), Inverse estimates of anthropogenic carbon uptake, transport, and storage by the ocean, *Global Biogeochem. Cycles*, *20*, GB2002, doi:10.1029/2005GB002530.

Milliman, J. D. (1993), Production and accumulation of calcium carbonate in the ocean: Budget of a nonsteady state, *Global Biogeochem. Cycles*, *7*(4), 927–957.

Milliman, J. D., and A. W. Droxler (1996), Neritic and pelagic carbonate sedimentation in the marine environment: Ignorance is not bliss, *Geol. Rundsch.*, *85*, 496–504.

Milliman, J. D., P. J. Troy, W. M. Balch, A. K. Adams, Y.-H. Li, and F. T. Mackenzie (1999), Biologically mediated dissolution of calcium carbonate above the chemical lysocline?, *Deep Sea Res., Part I*, *46*, 1653–1669.

Moore, J. K., S. C. Doney, J. A. Kleypas, D. M. Glover, and I. Y. Fung (2002), An intermediate complexity marine ecosystem model for the global domain, *Deep Sea Res., Part II*, *49*, 403–462.

Moore, J. K., S. C. Doney, and K. Lindsay (2004), Upper ocean ecosystem dynamics and iron cycling in a global three-dimensional model, *Global Biogeochem. Cycles*, *18*, GB4028, doi:10.1029/2004GB002220.

Murnane, R. J., J. L. Sarmiento, and C. LeQuéré (1999), The spatial distribution of air-sea fluxes and the interhemispheric transport of carbon by the oceans, *Global Biogeochem. Cycles*, *13*(2), 287–305.

Najjar, R., and J. C. Orr (1998), Design of OCMIP-2 simulations of chlorofluorocarbons, the solubility effects and common biogeochemistry, report, Ocean Carbon-Cycle Model Intercomparison Proj., Gif-sur-Yvette, France.

Najjar, R. G., J. L. Sarmiento, and J. R. Toggweiler (1992), Downward transport and fate of organic matter in the ocean: Simulations with a general circulation model, *Global Biogeochem. Cycles*, *6*(1), 45–76.

Nelson, D. M., P. Treguer, M. A. Brzezinski, A. Leynaert, and B. Quequiner (1995), Production and dissolution of biogenic silica in the ocean: Revised global estimates, comparison with regional data and relationship to biogenic sedimentation, *Global Biogeochem. Cycles*, *9*(3), 359–372.

Nelson, D. M., et al. (2002), Vertical budgets for organic carbon and biogenic silica in the Pacific sector of the Southern Ocean, 1996–1998, *Deep Sea Res., Part II*, *49*, 1645–1674.

Paasche, E. (1998), Roles of nitrogen and phosphorus in coccolith formation in *Emiliania huxleyi* (Prymnesiophyceae), *Eur. J. Phycol.*, *33*, 33–42.

Paasche, E. (1999), Reduced coccolith calcite production underlight-limited growth: A comparative study of three clones of *Emiliania huxleyi* (Prymnesiophyceae), *Phycologia*, *38*, 508–516.

Paasche, E. (2002), A review of the coccolithophorid *Emiliania huxleyi* (Prymnesiophyceae), with particular reference to growth, coccolith formation, and calcification-photosynthesis interactions, *Phycologia*, *40*, 503–529.

Pondaven, P., O. Ragueneau, P. Treguer, A. Hauvespre, L. Dezileau, and J. Reyss (2000), Resolving the "opal paradox" in the Southern Ocean, *Nature*, *405*, 168–172.

Ragueneau, O., et al. (2000), A review of the Si cycle in the modern ocean: Recent progress and missing gaps in the application of biogenic opal as a paleoproductivity proxy, *Global Planet. Change*, *26*, 317–365.

Ragueneau, O., N. Dittert, P. Pondaven, P. Treguer, and L. Corrin (2002), Si/C decoupling in the world ocean: Is the Southern Ocean different?, *Deep Sea Res., Part II*, *49*, 3127–3154.

Robbins, P. E. (2001), Oceanic carbon transport carried by freshwater divergence: Are salinity normalizations useful?, *J. Geophys. Res.*, *106*, 30,939–30,946.

Sarmiento, J. L., J. P. Dunne, A. Gnanadesikan, R. M. Key, K. Matsumoto, and R. Slater (2002), A new estimate of the $CaCO_3:C_{org}$ ratio, *Global Biogeochem. Cycles*, *16*(4), 1107, doi:10.1029/2002GB001919.

Sarmiento, J. L., N. Gruber, M. A. Brzezinski, and J. P. Dunne (2004a), High-latitude controls of thermocline nutrients and low-latitude biological productivity, *Nature*, *427*, 56–60.

Sarmiento, J. L., et al. (2004b), Response of ocean ecosystems to climate warming, *Global Biogeochem. Cycles*, *18*, GB3003, doi:10.1029/2003GB002134.

Sathyendranath, S., L. Watts, E. Devred, T. Platt, C. Caverhill, and H. Maass (2004), Discrimination of diatoms from other phytoplankton using ocean-colour data, *Mar. Ecol. Prog. Ser.*, *272*, 59–68.

Schlitzer, R. (2002), Carbon export fluxes in the Southern Ocean: Results from inverse modeling and comparison with satellite-based estimates, *Deep Sea Res., Part II*, *49*, 1623–1644.

Subramaniam, A., C. Brown, R. Hood, E. Carpenter, and D. Capone (2002), Detecting *Trichodesmium* blooms in SeaWiFS imagery, *Deep Sea Res., Part II*, *49*, 107–121.

Takeda, S. (1998), Influence of iron availability on nutrient consumption ratio of diatoms in oceanic waters, *Nature*, *393*, 774–777.

Usbeck, R. (1999), Modeling of marine biogeochemical cycles with an emphasis on vertical particle fluxes, Ph.D. thesis, 105 pp., Univ. of Bremen, Bremen, Germany.

Usbeck, R., R. Schlitzer, G. Fischer, and G. Wefer (2003), Particle fluxes in the ocean: Comparison of sediment trap data with results from inverse modeling, *J. Mar. Syst.*, *39*, 167–183.

Veldhuis, M. J., and G. W. Kraay (2004), Phytoplankton in the subtropical Atlantic Ocean: Towards a better assessment of biomass and composition, *Deep Sea Res., Part I*, *51*, 507–530, doi:10.1016/j.dsr.2003.12.002.

R. A. Armstrong, Marine Sciences Research Center, Stony Brook University, Stony Brook, NY 11794, USA. (rarmstrong@notes.cc.sunysb.edu)

J. P. Dunne, NOAA Geophysical Fluid Dynamics Laboratory, PO Box 308, Forrestal Campus B Site, Princeton, NJ 08542-0308, USA. (john.dunne@noaa.gov)

N. Gruber and X. Jin, Institute of Geophysics and Planetary Physics, University of California, Los Angeles, Los Angeles, CA 90095, USA. (xjin@igpp.ucla.edu; ngruber@igpp.ucla.edu)

J. L. Sarmiento, Atmospheric and Oceanic Sciences Program, Princeton University, Sayre Hall, Forrestal Campus, P.O. Box CN710, Princeton, NJ 08544-0710, USA. (jls@princeton.edu)